

Liquid Structure of 1-Ethyl-3-methylimidazolium Alkyl Sulfates by X-ray Scattering and Molecular Dynamics

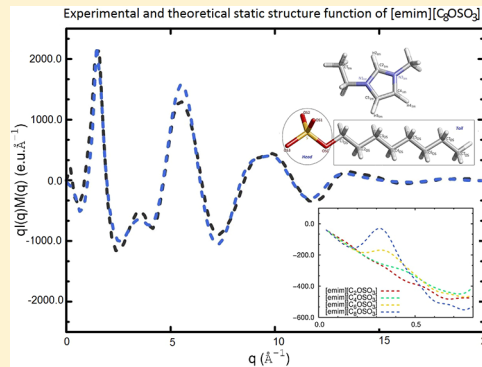
Marina Macchiagodena,*[†] Fabio Ramondo,*[†] Alessandro Triolo,*[‡] Lorenzo Gontrani,*[¶] and Ruggero Caminiti*,[¶]

[†]Department of Physical and Chemical Sciences, University of L'Aquila, Italy

[‡]Istituto Struttura della Materia, Consiglio Nazionale delle Ricerche, Rome, Italy

[¶]Department of Chemistry, University of Rome "Sapienza", P. le Aldo Moro 5, I 00185 Rome, Italy

ABSTRACT: We report a joined X-ray diffraction and molecular dynamics study on the series of 1-ethyl-3-methylimidazolium alkyl sulfates (alkyl = ethyl, butyl, hexyl, octyl) ionic liquids. A general good agreement between experimental and theoretical structure functions has been found for each term of the series in all ranges of q values. Once the quality of the employed force field in reproducing structural data was tested, we used dynamics simulations to access information on morphology and properties of these systems. The series of ionic liquids presents nanoscale structural heterogeneity, whose size depends on the anion alkyl chain length. Analyzing our simulation data on the basis of alkyl chain length, we propose a structural model consistent with the presence of low q peaks.



INTRODUCTION

Ionic liquids (ILs) are a class of useful and interesting materials for a variety of both scientific and applicative issues.^{1–3} They have found use in many laboratory as well as industrial applications spanning from electrochemistry⁴ to synthetic⁵ and catalytic chemistry.⁶ The high number of available cation–anion combinations allows, by changing the nature of ionic species or varying the alkyl chain length, to achieve ionic liquids with high tunable chemical physical properties.

A family of particularly promising ionic liquids is that of 1-ethyl-3-methylimidazolium [emim] alkyl sulfates [alkylOSO₃]. In 2002, Holbrey et al.⁷ proposed an easy and inexpensive halide-free manner of preparation of [emim] methyl sulfate and [emim] ethyl sulfate from the common industrial alkylating agent diethyl sulfate. Hereafter, a wide number of experimental studies has been devoted to the physical properties of 1-alkyl-3-methylimidazolium and sulfates with ethyl^{8–13} or longer alkyl chains.¹⁴ This class of ionic liquids is air and water stable, is water miscible, and has good thermal stability, low viscosity, and low toxicity. Since they are easily synthesized in an atom-efficient and halide-free way at a reasonable cost, such ionic liquids possess desirable properties for several industrial applications. To further expand the applications, ionic liquids-based mixed solvents have been proposed in recent years,¹⁵ and it has been shown that the presence of cosolvents such as water can affect the physical and chemical features of ionic liquids as well as solvation and solubility properties.^{16–18} Another important property concerns the role of the anion that acts as suppressor of protein aggregation and promotes in vitro refolding of denatured proteins. Renaturation yield is maximum

in the presence of 2(2-methoxyethoxy)ethyl sulfate, reduced with ethyl sulfate, whereas hexyl sulfate does not act as a refolding promoter at any tested concentration.¹⁹

Since structural organization might be responsible for several peculiar properties of these materials, their structure determination is a topic of great interest, although hardly straightforward. The development of atomistic simulation techniques and the parallel growth of computational power allow to reliably provide a nanoscopic interpretation of bulk properties of these materials.²⁰ Much progress has been made in the application of MD simulations to ionic liquids since the first study performed in 2001,²¹ and several force fields^{22–34} have been proposed so far. They were validated mainly on the basis of selected static and dynamic bulk properties and more recently also on the basis of X-ray (as well as neutron) diffraction data,^{35–43} one of the main sources of experimental information on liquid structure.

One of the peculiar structural aspects of ionic liquids emerging from several experimental evidences is the complexity of their mesoscopic spatial organization.^{44–50} This structural heterogeneity derives from the nature of two main interactions involving the different molecular moieties in the liquid, Coulombic interaction between charged groups, and dispersive interaction between apolar groups. Fully atomistic MD simulations provided structural insights of a nanoscale segregated morphology: in ionic liquids with highly sym-

Received: July 14, 2012

Revised: October 27, 2012

Published: October 29, 2012

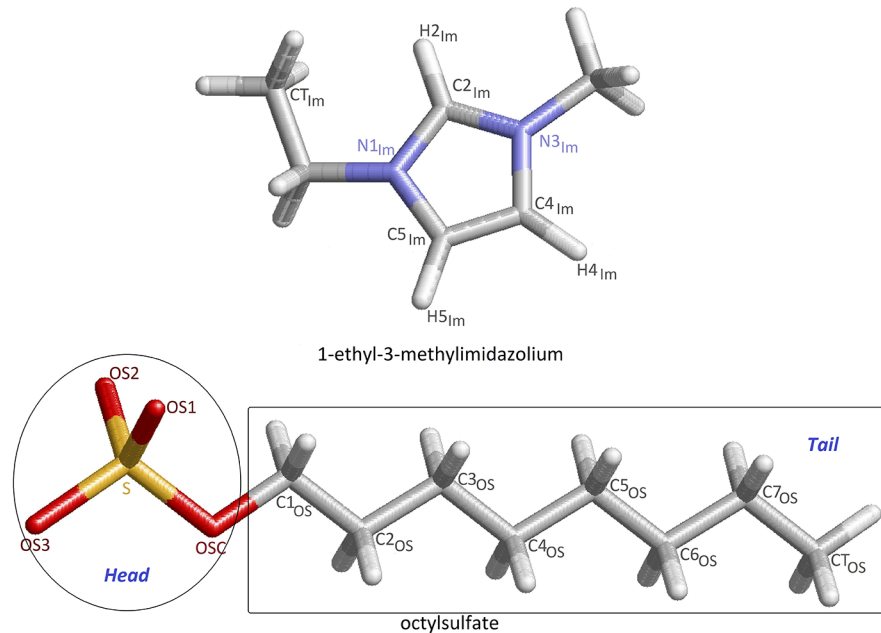


Figure 1. Atom labeling in 1-ethyl-3-methylimidazolium octylsulfate, [emim][C₈OSO₃].

metrical anions like PF₆⁻, the fluid structure is dominated by polar domains²² whereas with nonspherical anions, such as octyl sulfate, the nonpolar domains strongly permeate the liquid structure because the long alkyl chain may arrange efficiently.⁵¹ The effect of alkyl chain length on perturbation of polar domains seems to be greater when alkyl chain is connected to the anion.²² A synergic use of both theoretical and experimental techniques is therefore required to deeper describe this structural complexity and has been applied in this work.

Ionic liquids consisting of the 1-ethyl-3-methylimidazolium cation [C₂mim] combined with *n*-alkyl sulfate [C_{*n*}OSO₃] anions of the series *n* = 2 [C₂mim][C₂OSO₃], *n* = 4 [C₂mim][C₄OSO₃], *n* = 6 [C₂mim][C₆OSO₃], and *n* = 8 [C₂mim][C₈OSO₃] have been considered. Since their commercial names (from Solvent Innovation) are ECOENG 212, 214, 216, and 218, respectively, in the following we will identify these ILs as 212, 214, 216, and 218 for brevity. For atom labeling in 218, see Figure 1. This series of ionic liquids is characterized by an anion with a polar head bearing a well-localized negative charge and an alkyl tail of different length coupled with the same cation (1-ethyl-3-methylimidazolium) having a more diffuse ring charge distribution and a short ethyl chain. A comparative study of the various compounds in each series gives the opportunity to investigate how properties and structure of these liquids are affected by the alkyl chain length, as recently discussed in the complementary case where alkyl chain is linked to the imidazolium cation and anion is nearly spherical, PF₆⁻.^{43,52}

Chemical physical and structural properties of the [C₂mim] alkyl sulfates series were very recently investigated by some of us from density and refraction index measurements as well as small wide-angle X-ray scattering.¹⁴ A nanoscale structural heterogeneity was observed whose size was linearly dependent on the alkyl chain length.¹⁴ With the exception of [C₄mim]-[C₈OSO₃]⁵¹ and [C₂mim][C₂OSO₃]^{15,53} to our knowledge no atomistic MD simulations were instead carried out to study systematically these neat *n*-alkyl sulfates. Such previous investigations^{15,51,53} were carried out employing two different

force fields, the OPLS-AA one²⁵ parametrized for sulfate and sulfonate anions⁵⁴ and a force field derived from that originally proposed by Cadena and Maginn.³⁰ As for most MD studies, the accuracy of such force fields has been tested against a wide number of thermodynamic and transport properties of pure and water mixture ionic liquid; evidence about capability of such force fields in reproducing experimental diffraction data are instead still quite scarce. MD simulations are therefore here proposed on the basis of these two force fields, and the corresponding equilibrium structure has been compared with the findings from X-ray diffraction experiments.

The paper is organized as follows. In the first section, the first member of the series, [C₂mim][C₂OSO₃], has been studied employing both force fields^{15,54} and deriving static properties, such as density, vaporization enthalpy, and structural features along with dynamic properties, such as diffusive behavior. Then the force fields have been employed to calculate theoretical structure functions and compare them with the experimental functions. In the second section, the theoretical and experimental diffraction data have been compared for the remaining alkyl sulfates by employing one of two force fields.

EXPERIMENTAL DETAILS

1-Ethyl-3-methylimidazolium *n*-alkyl sulfate, [C₂mim]-[C_{*n*}OSO₃] (*n* = 2, 4, 6, 8), produced from Solvent Innovation, and commercialized as ECOENG 212, 214, 216 and 218, respectively, was treated as described in ref 14.

The large-angle X-ray scattering experiments were performed using the noncommercial energy-scanning diffractometer built in the Department of Chemistry at the University La Sapienza of Rome (patent no. 01126484, 23 June 1993). Detailed description of instrument, technique, and the experimental protocol (instrument geometry and scattering angles) of the data acquisition phase can be found elsewhere.^{55–60} The appropriate measuring time (i.e., number of counts) was chosen to obtain scattering variable (*q*) spectra with high signal-to-noise ratio (600 000 counts on average).

The expression of *q* is

$$q = \frac{4\pi \sin(\theta)}{\lambda} = 1.014E \sin(\lambda) \quad (1)$$

where E is expressed in keV and q in \AA^{-1} . The various angular data were processed according to the procedure described in the literature,^{55–60} normalized to a stoichiometric unit of volume containing one ionic couple and combined to yield the total “(static) structure function”, $I(q)$

$$I(q) = I_{\text{eu}}(q) - \sum_{i=1}^N x_i f_i^2 \quad (2)$$

where f_i are the atomic scattering factors, x_i are the number concentrations of the i -type atoms in the stoichiometric unit (i.e., the group of particles used as reference for data normalization, the ion pair in this case), and I_{eu} is the observed intensity in electron units (electrons²). This function was multiplied by q and q -dependent sharpening factor, $M(q)$, with nitrogen as the sharpening atom. This procedure enhances the resolution of the curve at high q values and decreases the truncation error in the calculation of the Fourier transform from reciprocal (q) to direct space (r). Fourier transform of $I(q)$ led to radial distribution function (RDF)

$$D(r) = 4\pi r^2 \rho_0 + \frac{2r}{\pi} \int_0^{q_{\max}} q I(q) M(q) \sin(rq) dq \quad (3)$$

where ρ_0 (electrons²/ \AA^3) is the bulk number density of stoichiometer units. When the uniform distribution component is dropped ($4\pi r^2 \rho_0$), we obtain the differential correlation function, $\text{Diff}(r)$, which contains only the structural contribution to the distribution function

$$\text{Diff}(r) = D(r) - 4\pi r^2 \rho_0 \quad (4)$$

COMPUTATIONAL DETAILS

Molecular dynamics simulations of $[\text{C}_2\text{mim}][\text{C}_n\text{OSO}_3]$ ($n = 2, 4, 6, 8$) were performed using the DL-POLY package.^{61,62} The ILs were simulated in periodic cubic boxes of edge shown in Table 1 containing 729 ion pairs for 212 and 214 and 1000 for

Table 1. Theoretical ρ_{MD} and Experimental ρ_{exp} Density (g/cm³) of 212, 214, 216, and 218 Liquids^g

sample	ρ_{MD}		ρ_{exp}
	CLAP (KSM)	T = 298.15 K	box edge (Å)
212	1.24 (1.24)	1.2369 ^a ; 1.2296 ^b ;	
		1.2430 ^c ; 1.23763 ^d ;	
		1.23692 ^e ; 1.23733 ^f	61.32900
214	1.18	1.1763 ^a	64.72750
216	1.13	1.1304 ^a	74.46020
218	1.10	1.0947 ^a	78.50107

^aReference 14. ^bReference 64. ^cReference 65. ^dReference 66.

^eReference 67. ^fReference 68. ^gFor *a*, *b*, and *c* uncertainty is $\pm 10^{-4}$; for *d*, *e*, and *f* $\pm 10^{-5}$.

216 and 218. Initial low-density configurations, with ions placed randomly in periodic cubic boxes, were equilibrated to obtain liquidlike densities and structures at 298 K and 1 atm. Temperature and pressure were maintained using a Nosé–Hoover thermostat and barostat, respectively. Once the equilibrium density was obtained, simulations runs of 5 ns with a time steps = 2 fs, in NVT ensemble, were performed. Nonbonded interactions were computed up to 8 Å, and

theoretical structure factors $I(q)$ were calculated (out of 5000 configurations stored during the simulation progress) using the following equation⁶³

$$I(q) = \sum_{i=1}^N \sum_{j=1}^N x_i x_j f_i f_j H_{ij}(q) \quad (5)$$

$H_{ij}(q)$ are the partial structure factors, defined in terms of the radial distribution functions by the Fourier integral

$$H_{ij}(q) = 4\pi \rho_0 \int_0^{r_{\max}} r^2 (g_{ij}(r) - 1) \frac{\sin(qr)}{qr} dr \quad (6)$$

where r_{\max} is the half the box edge. The partial structure factors and the theoretical structure factors have been calculated with an in-house written code. Theoretical $I(q)$ was then multiplied by q and the sharpening factor, $M(q)$, to obtain a theoretical $qI(q)M(q)$ function that directly compares with experimental $I(q)$. Theoretical $\text{Diff}(r)$ functions were also calculated as described above for experimental ones.

RESULTS AND DISCUSSION

Two Force Fields in Comparison. In order to evaluate the dependence of the calculated properties from force field, MD simulations were carried out first on $[\text{C}_2\text{mim}][\text{C}_2\text{OSO}_3]$ employing two force fields recently developed for this class of ionic liquids: one potential was parametrized for sulfate and sulfonate anions⁵⁴ starting from the OPLS-AA one²⁵ (hereafter indicated as CLAP), and a second potential was proposed by Kelkhar, Shin, and Maginn¹⁵ for $[\text{C}_2\text{mim}][\text{C}_2\text{OSO}_3]$ (hereafter indicated as KSM). The performance of such models was first tested against the liquid density as shown in Table 1. The values obtained by both force fields from NVT simulations are substantially equal and in agreement with most experimental data. This is not surprising since it has already observed that different force fields often yield similar density.¹⁵

The molar enthalpy of vaporization at 1 atm pressure was then calculated by the expression $\Delta H_{\text{vap}}(T, P) = \langle U_{\text{gas}}(T) \rangle + RT - \langle U_{\text{liq}}(T, P) \rangle - PV_{\text{liq}} U_{\text{liq}}(T, P)$ is the ensemble average molar configurational energy obtained from simulation for liquid whereas $U_{\text{gas}}(T)$ was derived assuming vapor phase consisting of isolated molecules in the NVT ensemble and simulating it for the same time of liquid. The values obtained at 298.15 K are 208 kJ mol⁻¹ for CLAP and 192 kJ mol⁻¹ for KSM (Table 2). Unfortunately, no experimental values are reported in the literature to our knowledge to evaluate the accuracy of these results.

For each of the runs carried out by CLAP and KSM force fields, radial distribution functions (RDFs) representative of the cation anion distribution, $g_{\text{OS}\cdots\text{H}_2\text{Im}}(r)$ and $g_{\text{OS}\cdots\text{H}_4\text{Im}}(r)$, ($\text{OS}\cdots\text{HS}_{\text{Im}}$) were calculated (OS are the undifferentiated oxygen atoms indicated as OSX, with X = 1–3 in Figure 1). As shown in Figure 2b, CLAP and KSM potentials reproduce

Table 2. Molar Vaporization Enthalpy ΔH_{vap}^0 (298.15K)(kJ/mol) Obtained for 212, 214, 216, and 218 Liquids from MD

sample	ΔH_{vap}^0 (CLAP)
212	208 (192) ^a
214	201
216	218
218	232

^aIn parentheses the KSM value is reported.

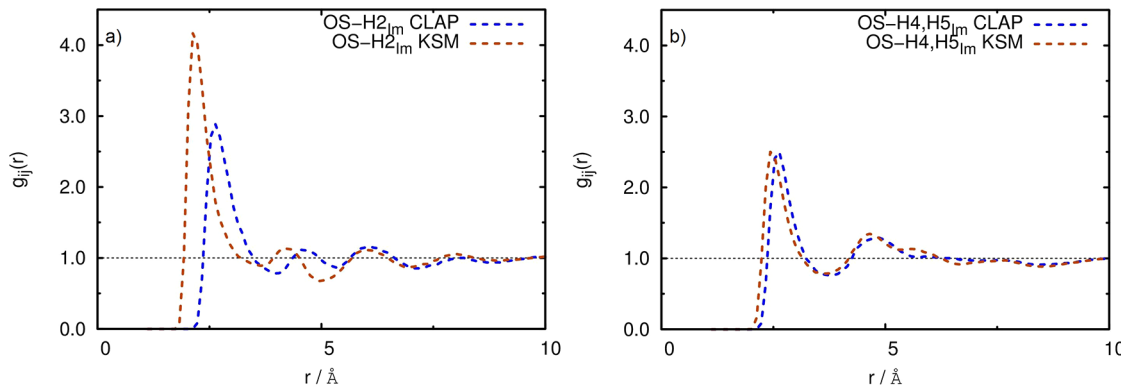


Figure 2. Radial distribution function between oxygen atom, OS, and hydrogen cation atoms, $H_{2\text{Im}}$, $H_{4\text{Im}}$, $H_{5\text{Im}}$ ($H_{S\text{Im}}$) in $[\text{emim}][\text{C}_2\text{OSO}_3]$.

similarly the $\text{OS}\cdots\text{H}_{4\text{Im}}(\text{H}_{5\text{Im}})$ interaction in position and intensity. Some differences are instead found for the favorite interaction site (Figure 2a): KSM's $g_{\text{OS}\cdots\text{H}_{2\text{Im}}}$ principal peak (centered at ca. 2.4 \AA) is more intense, and it occurs at smaller r values than that found using the CLAP potential. Comparing then all $g_{\text{OS}\cdots\text{H}_{\text{Im}}}(r)$ couples, we found indeed similar $\text{OS}\cdots\text{H}_{\text{Im}}$ interactions using CLAP; small discrepancies were instead observed by KSM. This is probably due to the different charges attributed to hydrogen ($\text{H}_{2\text{Im}}$, $\text{H}_{4\text{Im}}$, $\text{H}_{5\text{Im}}$) atoms in KMS potential.

Another important test for force field is its capability of reproducing diffusive conditions. To check if the system is in diffusive regime,²⁰ $\log(\text{MSD})$ against $\log(t)$ was reported in Figure 3. Marked deviations from pure diffusive behavior have

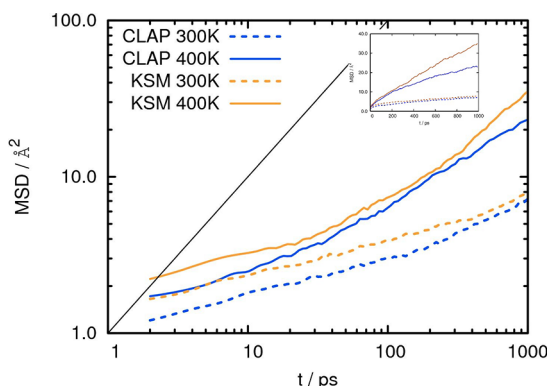


Figure 3. Comparison of MSD for all atoms obtained with CLAP and KSM force fields. In the inset is linear scale.

been found for both force fields at $T = 300 \text{ K}$ as well as $T = 400 \text{ K}$. As expected, the curves slope increases with temperature; however, its value is yet far from that expected in diffusive regime. As a matter of fact ionic liquids are very viscous, and in order to reach diffusive conditions, one needs very long simulations;⁶⁹ however, the size of such systems does not allow to further increase times of our simulation. Presumably, also diffusive coefficient derived for $[\text{C}_4\text{mim}][\text{C}_8\text{OSO}_3]$ by Leal et al.⁵¹ could be affected by the limited duration of the simulation. One of the reasons of the scarce capability in reproducing diffusion of both force fields could be found in the tendency to overestimate the cation anion interaction. This could trap ions in local stable structures which hinder diffusion. As a proof, the KSM force field which assumes lower charges for hydrogen, oxygen, and ring atoms leads to higher MSD values. This is

consistent also with the lower vaporization enthalpy (Table 1) obtained with the KSM potential.

On the other hand, it is well-known that accurate predictions of transport properties could be obtained only with polarizable force fields. For unpolarized force fields, Bhargava and Balasubramanian⁷⁰ showed that the diffusive conditions are well reproduced for some ionic liquids when the total charge of ionic species is lowered.

Lastly the structure function $qI(q)M(q)$ was calculated with the two force fields and compared with the experimental function in Figure 4 where we report data in the q range 0–10

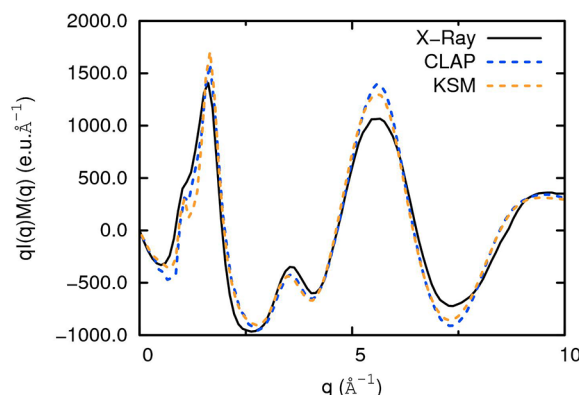


Figure 4. Comparison of $qI(q)M(q)$ for $[\text{emim}][\text{C}_2\text{OSO}_3]$ calculated with CLAP and KSM force field.

\AA^{-1} to better visualize the differences between the various curves. Figure 4 shows that CLAP and KSM force fields reproduce reasonably the experimental data, with a slightly better agreement in the low q region for CLAP. On the basis of previous considerations we can conclude that both potentials yield comparable values for important properties of $[\text{emim}][\text{C}_2\text{OSO}_3]$. As concerning structural features, the CLAP force field seems to reproduce slightly better the low q portion of the ($0\text{--}2.5 \text{ \AA}^{-1}$) structure function, and therefore we decided to employ this potential to simulate all liquids of the series. In addition, all systems were simulated at 500 K to increase the mobility of liquids as well as to improve the accuracy of the theoretical model in the whole q range of the structure function.

1-Ethyl-3-methylimidazolium Alkyl Sulfates. All systems were simulated in the NVT ensemble, and the same properties discussed for the first element of the series (212) were calculated for the remaining compounds. As for 212, our

simulations well reproduce the measured density (see Table 1) of all liquids. Along with density, the molar enthalpy of vaporization (Table 2) was calculated, and its value, as expected, increases with the size of alkyl chain.

The static structure function $I(q)$ derived from molecular dynamics is then compared with the corresponding experimental functions for 212 in Figure 5a, 214 in Figure 6a, 216 in

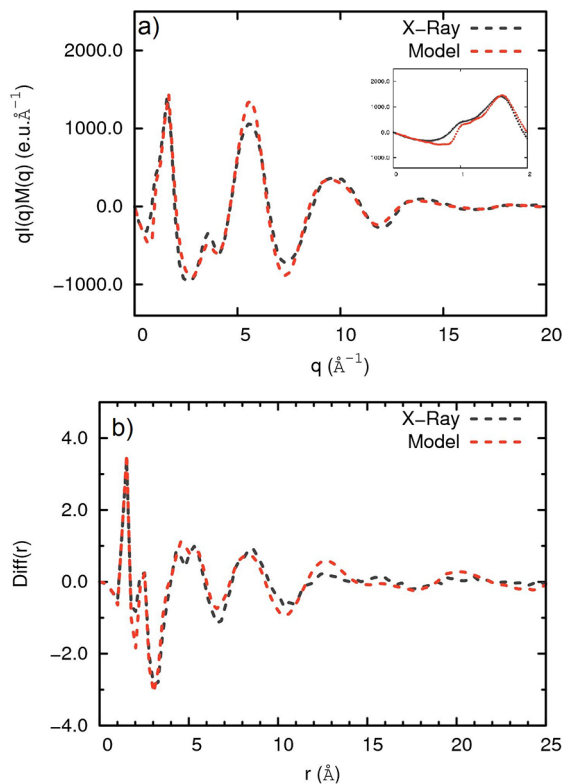


Figure 5. Experimental and theoretical $qI(q)M(q)$ (a) and $\text{Diff}(r)$ (b) of $[\text{emim}][\text{C}_2\text{OSO}_3]$. In the inset the low q portion is reported.

Figure 7a, and 218 in Figure 8a. For each molecular species the radial distribution functions, $\text{Diff}(r)$, are also reported in Figures 5b, 6b, 7b, and 8b. A first point emerging from such a comparison is the general good agreement between model and experiment for all the liquids, thus supporting the quality of the employed force field. The second important result is that the experimental static structure functions of 216 and 218, the systems with longer alkyl chain, show a typical feature at low q values already observed by Triolo et al.¹⁴ The presence of such low q peaks and their dependence from the alkyl tail length were interpreted as an indication of a degree of mesoscopic order.⁴⁴

We are aware that our box dimension is not adequate to reproduce accurately the low q peak's intensity; however, the box length is significantly larger than critical values ($4\pi/q$) for all members of the series. In addition Margulis's study⁷¹ showed that intensity and not position of the low q peak could change beyond critical distances. On the other hand, only slight improvements were observed enlarging one of the box dimensions.⁴³ We therefore argue that it is worth exploring anyway such region in the theoretical curves. It is very interesting to note that our simulations predict indeed low q peaks for 218 and, although at very low intensity, also for 216. These features in the static structure functions are reflected in the relative radial distribution functions from which we note

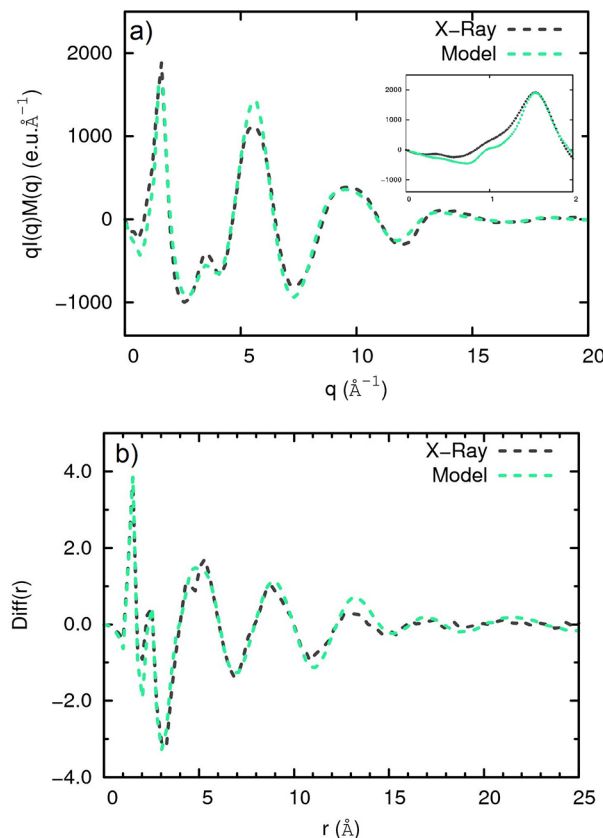


Figure 6. Experimental and theoretical $qI(q)M(q)$ (a) and $\text{Diff}(r)$ (b) of $[\text{emim}][\text{C}_4\text{OSO}_3]$. In the inset the low q portion is reported.

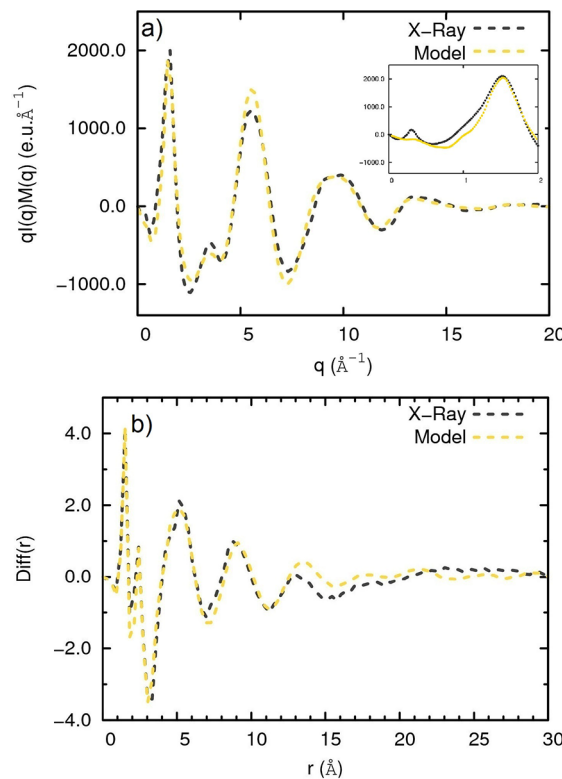


Figure 7. Experimental and theoretical $qI(q)M(q)$ (a) and $\text{Diff}(r)$ (b) of $[\text{emim}][\text{C}_6\text{OSO}_3]$. In the inset the low q portion is reported.

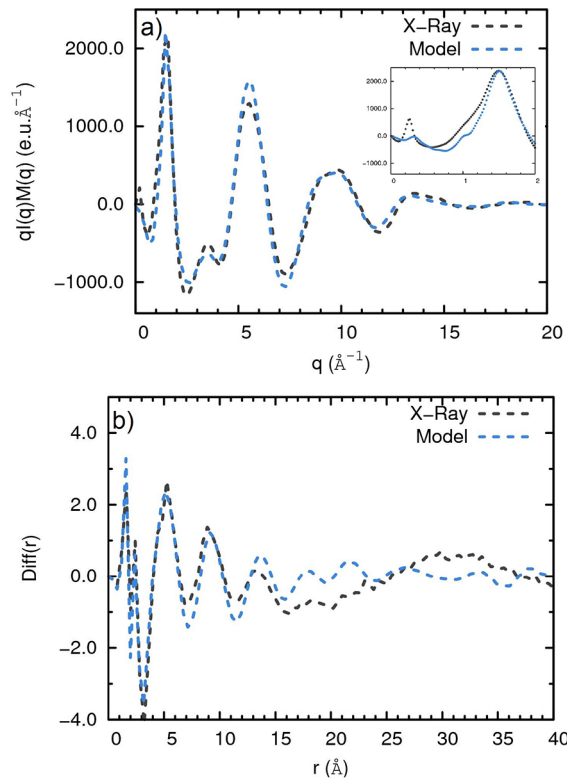


Figure 8. Experimental and theoretical $qI(q)M(q)$ (a) and $Diff(r)$ (b) of $[\text{emim}][\text{C}_8\text{OSO}_3]$. In the inset the low q portion is reported.

that liquids with longer alkyl chains show more ordered structures. As a matter of fact such long-range order seems to emerge better from theoretical than experimental curves, especially for 218 (Figure 8b). Discrepancies between theory and experiment could be originated again from the low efficiency of force field in reproducing mobility of ionic species in the liquid, particularly for long anions such as 218. However, a general good agreement is observed below 15 \AA for all members of the series.

Effects of alkyl chain are appreciable in the whole range of static structure function: as for the low q peak, also main peaks at 1.5 and 5.5 \AA^{-1} are size chain dependent and are more intense for 218. Consistently, the regions of $Diff(r)$ at higher r values are sensitive to the molecular size: the two peaks measured around 5.2 \AA for the shortest chain, 212, coalesce in a single and more intense signal for the longest chain, 218. Changes are also observed in the region at about 10 \AA .

Static Structure Function: Contributions. With the aim to rationalize the changes of $I(q)$ or $Diff(r)$ in the four investigated systems, we factorized the total static structure function into partial contributions separating first the cation from anion contribution. The cation partial function was further factorized into intramolecular and intermolecular terms, whereas from the anion contribution we distinguished a term describing head–head interactions (polar–polar) and a second one containing tail–tail (nonpolar–nonpolar) interactions. Cation–anion and anion tail–anion head terms were derived by difference between previous contributions. All intermolecular contributions are shown in Figure 9 for the longest alkyl chain salt focusing attention on the low q region where two peaks at 0.9 and 1.5 \AA^{-1} along with the prepeak at 0.3 \AA^{-1} are found. Figure 10 reports how each contribution changes in the series 212–218 in the same q region.

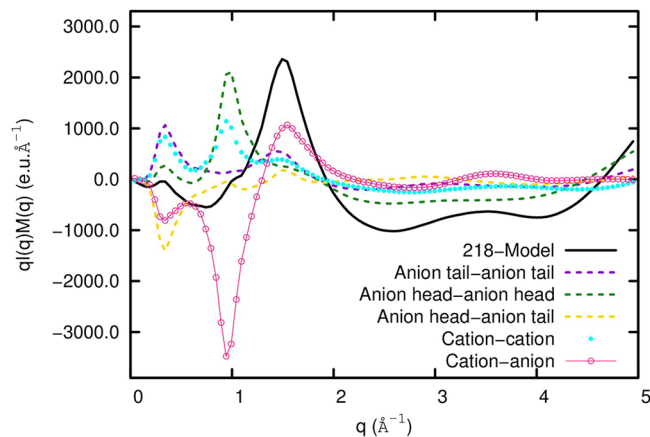


Figure 9. Contributions for structure function of $[\text{emim}][\text{C}_8\text{OSO}_3]$.

Inspection of Figure 9 reveals that 0.9 \AA^{-1} peak is dominated positively by polar–polar (anion head–anion head) term and negatively by cation–anion term. This is expected for the charge-ordering peaks around 0.9 \AA^{-1} , as already observed for $[\text{C}_n\text{mimBr}]$,⁷² $[\text{C}_6\text{mimCl}]$,⁷¹ and $[\text{C}_n\text{mimPF}_6]$.⁴³ Cross-term (cation–anion) and nonpolar (anion tail–anion tail) contributions play a significant role for 1.5 \AA^{-1} peak.

All intermolecular terms contribute, positively or negatively, to the 0.3 \AA^{-1} peak. In particular the positive peaks coming from anion–anion contributions (polar head–head, Figure 10b, and nonpolar tail–tail, Figure 10a) are balanced by the negative peak of polar–nonpolar (anion head–anion tail, Figure 10c) term. The resulting anion–anion term vanishes (Figure 10f), and a net positive contribution comes only from cation–cation interactions (Figure 10d). In addition each contribution changes from 212 to 218. For the low q peak, an increase occurs for tail–tail, head–head anion, and cation–cation terms whereas a decrease is found for head–tail and cation–anion terms. For the remaining peaks a lower size chain effect is observed. On the ground of these partial contributions, it emerges that the low q peak seems to be dominated from a cation–cation term which becomes more intense and moves to lower q values with increase of alkyl chain. This effect has been already observed by Hardacre,⁵² Margulis,⁷¹ Aoun,⁷² and Triolo⁴³ when alkyl chains are linked to the cation.

From patterns of Figure 10 we can therefore conclude that the low q peak mainly stems from the contribution of imidazolium head–head although also the anion tail–anion tail term plays an important role and could be responsible for the alkyl size dependence of the peak. A structural model consistent with this trend predicts a spatial distribution where cations, interacting with anions bearing alkyl chains progressively longer, are more distant from each other with increasing of the anion size. In Figure 11 we report a possible feature obtained from some snapshots of the trajectory which shows the arrangement of some cations in 212 (Figure 11a) and 218 (Figure 11b). As a matter of fact distances between cations may depend on the degree of interdigitation of the alkyl chains. By estimating the cation–cation separation from geometries of force field, we expect a value within 35–25 \AA for 218 and 18–16 \AA for 212. Associated with such correlation length we predict a q range of 0.18–0.25 \AA^{-1} (218) and 0.35–0.4 \AA^{-1} (212) not far from the experimental 0.31 \AA^{-1} (218) and 0.40 \AA^{-1} (212) peaks. The proposed structure could be therefore the result of synergic effects which start from the

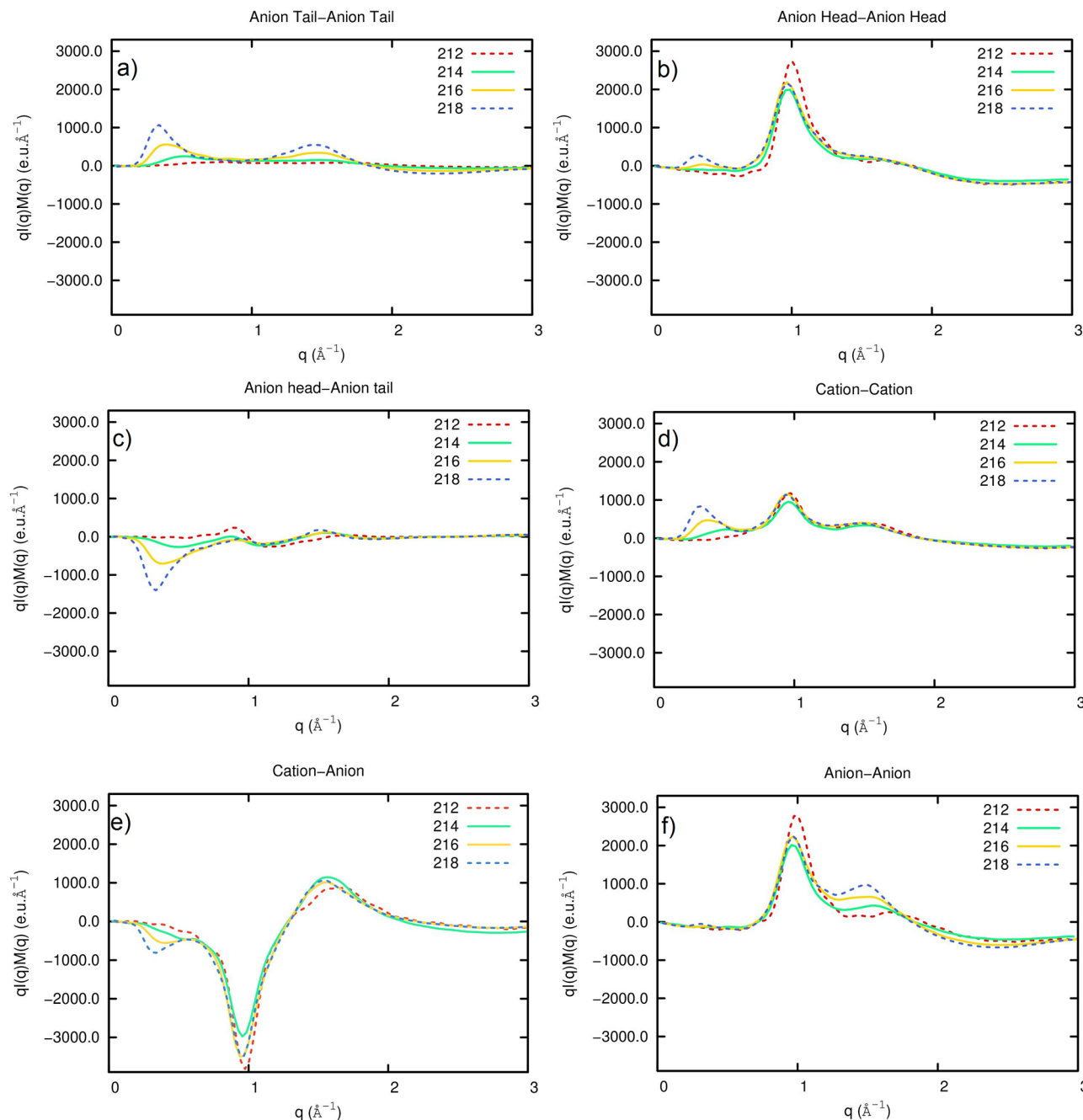


Figure 10. (a) Anion tail–anion tail; (b) anion head–anion head; (c) anion head–anion tail; (d) cation–cation; (e) cation–anion; (f) anion–anion contribution in the series.

favorable orientation between polar anion heads and polar cations, contribution cation–anion at 1.5 \AA^{-1} and corresponding to a correlation length of 4.2 \AA . Negative heads avoid each other by repulsive interactions (peak at 0.9 \AA^{-1}), whereas alkyl portions, driven by dispersion interactions, approach each other (peak at 1.5 \AA^{-1}). In conclusion, the concerted effect of aggregation between alkyl tails and repulsion between negative heads might force an alignment of anions between cationic positions as emerges from the microscopic local structure derived from some snapshots and reproduced in Figure 11c and d.

Structural Analysis. The structural model here proposed has been further tested by analyzing anion–cation as well as

alkyl chain distribution from partial radial distribution functions, $g(r)$.

Anion–Cation Distribution. Since cations and anions interact through OS1, OS2, and OS3 oxygen and H2_{Im} , H4_{Im} , HS_{Im} hydrogen atoms of the imidazolium ring, we analyzed the radial distribution functions between each oxygen and the H2_{Im} , H4_{Im} , HS_{Im} hydrogen atoms. The comparison between RDFs involving OS1, OS2, and OS3 revealed first the structural equivalence of the OS groups. In Figure 12 we report those relative to OS1, $g_{\text{OS1}} \cdots \text{H2}_{\text{Im}}(r)$, $g_{\text{OS1}} \cdots \text{H4}_{\text{Im}}(r)$, and $g_{\text{OS1}} \cdots \text{HS}_{\text{Im}}(r)$. The peaks' positions for the three functions is the same whereas their intensities indicate that H2_{Im} is the preferred interaction site with the oxygen. In addition in Figure 12 we report the radial distribution function between S and H

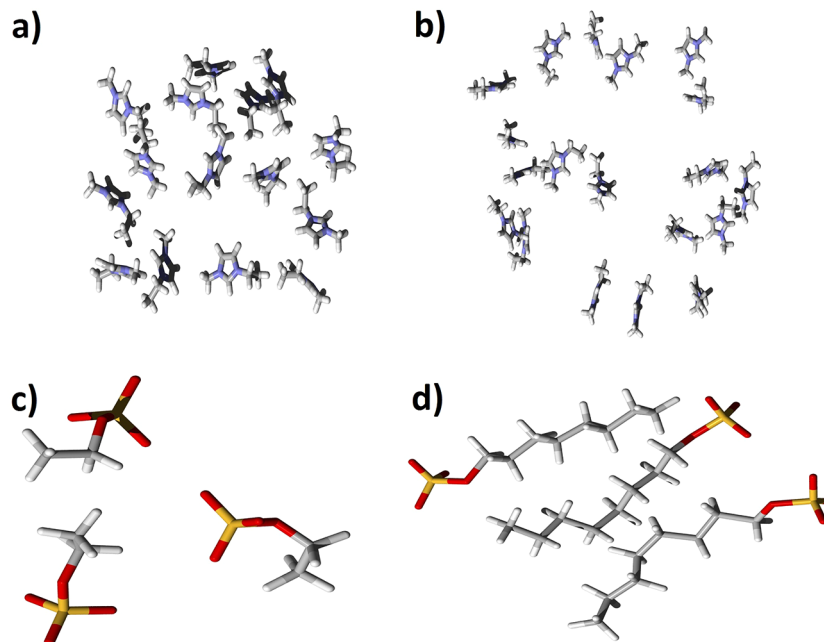


Figure 11. Local structure of 212 (a–c) and 218 (b–d) from selected snapshots of trajectory.

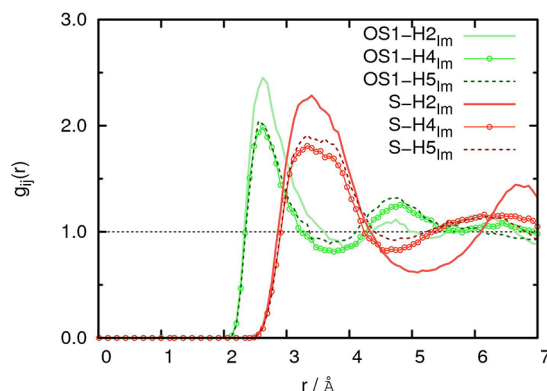


Figure 12. Radial distribution function between oxygen (OS1) and sulfur (S) anion atoms and hydrogen cation atoms ($H_{2\text{Im}}$, $H_{4\text{Im}}$, and $H_{5\text{Im}}$) in [emim][C₂OSO₃].

atoms, $g_{S\cdots H2\text{Im}}(r)$, $g_{S\cdots H4\text{Im}}(r)$, and $g_{S\cdots H5\text{Im}}(r)$. As expected, such functions are shifted at higher distances; however, the amount of the shift is lower than a SO bond

length adopted by force field (1.54 Å) suggesting that the $\angle SOH$ angle is far from linearity. The integration of each $g_{OS\cdots H\text{Im}}(r)$ up to the first minimum (4 Å) indicates that the number of first neighbors is close to one, thus revealing that each oxygen interacts with a single hydrogen atom. Integration of $g_{S\cdots H\text{Im}}(r)$ up to the first minimum (5 Å) indicates that each sulfur is surrounded by approximately five hydrogen atoms: the first shell centered at ca. 3.3 Å is built up by ca. three hydrogen atoms while another shell exists at ca. 4 Å with approximately two H atoms, which are presumably the neighbor atoms in position 4/5 with respect to the atoms in the first shell. Such distribution seems to be found in all the members of the series. Inspection of the $g_{S\cdots N1\text{Im}}(r)$ and $g_{S\cdots N3\text{Im}}(r)$ RDFs (data not shown) reveals that the anions approach N1 as well as N3 without preference in agreement with the similar steric hindrance of methyl and ethyl groups.

Alkyl Chain Distribution. The aim of this last section is to discern, using some carbon–carbon radial distribution functions, the existence of interactions between alkyl chains of the ionic species. To visualize the alkyl–alkyl distribution in

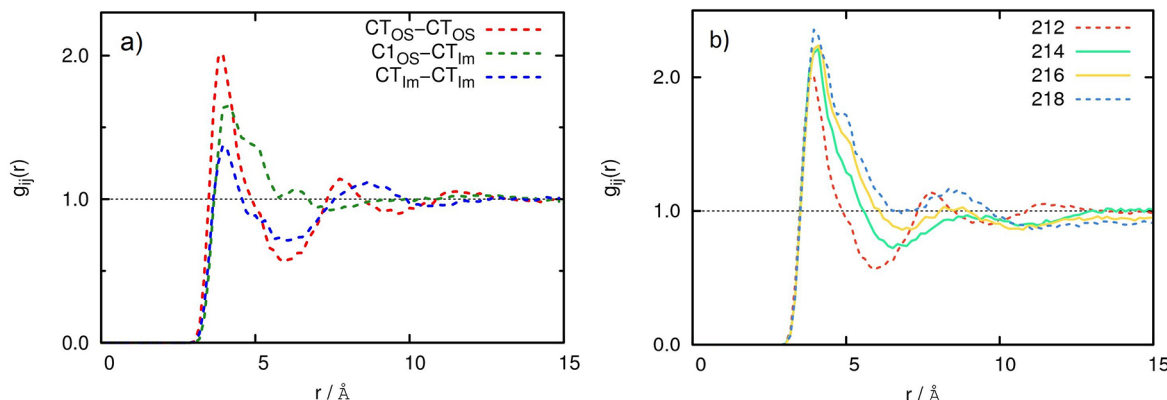


Figure 13. (a) Radial distribution function between the terminal carbon of the ethyl group CT_{Im} and the first and the terminal carbon of the alkyl chain, CT_{OS} and $C1_{\text{OS}}$; (b) radial distribution function between $CT_{\text{OS}}\cdots CT_{\text{OS}}$ in the series.

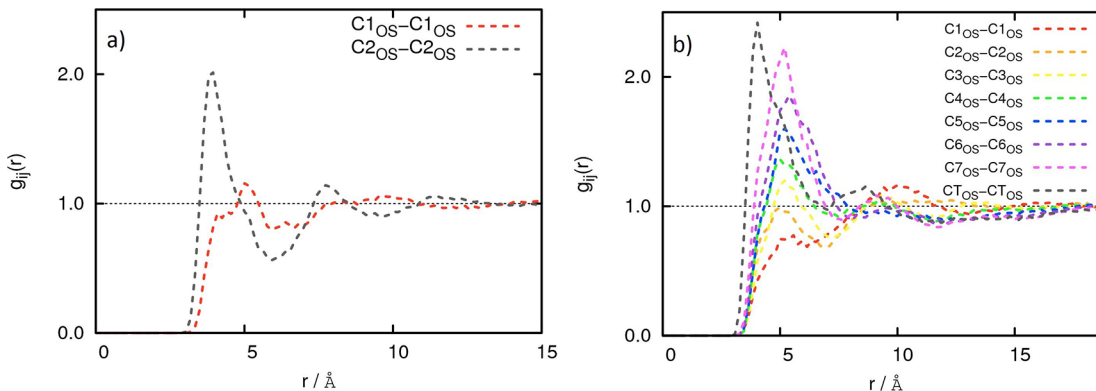


Figure 14. (a) Radial distribution function for alkyl chain in 212; (b) radial distribution function for alkyl chain in 218.

liquid, we considered all the pair RDFs between the terminal carbon of the ethyl group CT_{Im} , the first, $C1_{\text{OS}}$, and the terminal, CT_{OS} , carbon of the alkyl anion chain. Once observed that $g_{CT_{\text{Im}} \cdots CT_{\text{Im}}}(r)$ is almost the same for all the systems (data not shown), $g_{CT_{\text{Im}} \cdots CT_{\text{Im}}}(r)$, $g_{CT_{\text{Im}} \cdots C1_{\text{OS}}}(r)$, and $g_{CT_{\text{OS}} \cdots CT_{\text{OS}}}(r)$ functions were compared in Figure 13a for 212, the system where the anion and cation alkyl chains have similar length. The pattern of these RDFs is indicative of the presence of nonpolar domains involving alkyl chains of anions, cations, as well as anions–cations. Moreover, the shoulder at about 5 Å in $g_{CT_{\text{Im}} \cdots C1_{\text{OS}}}(r)$ RDF could be indicative of interdigitation between anion cation alkyl chains. For the remaining members of the series, a slight dependence on the chain length was found for the $g_{CT_{\text{Im}} \cdots C1_{\text{OS}}}(r)$ function (data not shown). Significant differences are instead noted in the series for $g_{CT_{\text{OS}} \cdots CT_{\text{OS}}}(r)$, and Figure 13b shows that for the longest chain, 218. For this liquid we expect a high number of contacts between alkyl portions (main peak 4 Å) although its structure appears more disordered than in other members of the series (shoulder at about 5 Å).

Reciprocal orientations of the alkyl chains can be revealed also from RDFs between internal carbons of the anion chain, and Figure 14a reports those for 212 and Figure 14b those for 218. For short chains, 212, the peak is well-defined only for terminal carbons, suggesting a quite random orientation of ethyl chains. However, this pattern does not exclude that also short chains could give origin to segregation in agreement with the presence of weak peaks at low q also in 212.¹⁴ For longer chains, 218, peaks are expected also from internal carbons, from $C7_{\text{OS}} \cdots C7_{\text{OS}}$ to $C3_{\text{OS}} \cdots C3_{\text{OS}}$, suggesting a interdigitating coordination between chains. Among all carbons, those terminal undoubtedly approach better each other, see Figure 14b), whereas the contributions at 5 Å are clearly correlated with the chain size. Once again we find that reciprocal organization of alkyl chain increases with size (Figure 11) and causes the appearance of the low q peak.^{14,44,46,50,71,73–77}

The conformation of the alkyl chains was last investigated through the study of angular distribution functions (ADFs) for some dihedral angles. For the cation, $C2_{\text{Im}}-\text{N}1_{\text{Im}}-\text{C}-CT_{\text{Im}}$, the dihedral angle which defines the orientation of the ethyl group with respect to the imidazolium plane assumes mainly $\pm 120^\circ$ (gauche conformation) and also 0° (coplanar conformation) values. For the anion we analyzed all the dihedral angles of the chain starting from that one, $OS-\text{S}-OCS-C1$, which defines the orientation of oxygen atoms in the sulfate group. Its values ($\pm 180^\circ$ and $\pm 60^\circ$) are the same in all the systems and indicate that sulfate is oriented to have oxygen

atoms equivalent in all liquids. The conformation about the $OSC-C1_{\text{OS}}$ bond, described by the second angle, $S-\text{OSC}-C1_{\text{OS}}-C2_{\text{OS}}$, is prevalently trans ($\pm 180^\circ$) with a minor alternative conformation ($\pm 95^\circ$) which tends to be negligible for long chain (218). This value, $\pm 95^\circ$, is determined by intramolecular interaction between OSC and CT hydrogen atom for 212. For the remaining angles, from $OSC-C1_{\text{OS}}-C2_{\text{OS}}-C3_{\text{OS}}$ to $C5_{\text{OS}}-C6_{\text{OS}}-C7_{\text{OS}}-CT_{\text{OS}}$, the curves indicate that the alkyl chain mostly assumes the all-trans conformation ($\pm 180^\circ$) along with a minor populated gauche ($\pm 65^\circ$) orientation. The relative abundance of gauche increases by moving toward the end of the chain suggesting a higher mobility of the terminal groups.

CONCLUSIONS

In this paper, X-ray diffraction data are presented on the series of 1-ethyl-3-methylimidazolium [emim] alkyl sulfates [alkylOSO₃]. For the first element of the series, molecular dynamics simulations were performed employing both the Lopes–Padua force field as well as the Cadena–Maginn one. Both models described bulk properties as well as X-ray diffraction data with similar accuracy. The remaining terms of the series were then calculated using the Lopes–Padua potential. A general good agreement between experimental and theoretical structure functions has been found for each term of the series in all ranges of q values. The systems with longer alkylic chain, 216 and 218, show features in the experimental structure functions at low q values already observed by Triolo et al. in previous investigations.¹⁴ Our simulations predict the presence of low q peaks for 218 and, although at very low intensity, also for 216. From radial distribution functions, extracted from MD simulations, important structural information was obtained. Features of radial distribution functions and microscopic local structures obtained from MD snapshots are indicative of the presence of nonpolar domains involving chains of the anions and cations. In conclusion, favorable orientations of two polar portions of the anion and cation, aggregation of alkyl tails, and repulsion of negative heads might force an alignment of anions between cationic positions. In addition analysis of the distribution of the alkyl chains shows that these are preferentially all-trans oriented along with a minor population for the gauche orientations.

AUTHOR INFORMATION

Corresponding Author

*E-mail: marina.macchiagodena@gmail.com (M.M.); fabio.ramondo@univaq.it (F.R.); triolo@ism.cnr.it (A.T.); l.gontrani@caspur.it (L.G.); r.caminiti@caspur.it (R.C.).

Notes

The authors declare no competing financial interest.

ACKNOWLEDGMENTS

Financial support from CASPUR (Centro di Applicazione di SuperCalcolo per Università e Ricerca—Rome Supercomputing Center)—Standard Grant 2011 std11-425 is acknowledged. M.M. thanks Dr. Enrico Bodo and Dr. Valentina Migliorati for the development of the codes to calculate the theoretical X-ray structure factors. A.T. acknowledges financial support from FIRB “Futuro in Ricerca” (RBFR086BOQ) and PRIN2009 (2009WPHRH).

REFERENCES

- (1) Wilkes, J. S. *Green Chem.* **2002**, *4*, 73–80.
- (2) Castner, E. W., Jr.; Wishart, J. F. *J. Chem. Phys.* **2010**, *132*, 120901–120909.
- (3) Wasserscheid, P.; Keim, W. *Angew. Chem., Int. Ed.* **2000**, *39*, 3772–3789.
- (4) Wasserscheid, P.; Keim, W. *Electrochemical Aspects of Ionic Liquids*; Wiley: Hoboken, NJ, 2005.
- (5) Wasserscheid, P.; Welton, T. *Ionic Liquids in Synthesis*; Wiley-VCH: Weinheim, Germany, 2003.
- (6) Parvulescu, V. I.; Hardacre, C. *Chem. Rev.* **2007**, *107*, 2615–2665.
- (7) Holbrey, J. D.; Reichert, W.; Swatloski, R. P.; Broker, G. A.; Pitner, W. R.; Seddon, K. R.; Rogers, R. D. *Green Chem.* **2002**, *4*, 407–413.
- (8) Torrecilla, J. S.; Rojo, E.; Garcia, J.; Rodriguez, F. *Ind. Eng. Chem. Res.* **2008**, *47*, 4025–4028.
- (9) Ficke, L. E.; Rodriguez, H.; Brennecke, J. F. *J. Chem. Eng. Data* **2008**, *53*, 2112–2119.
- (10) Gonzalez, E. J.; Gonzalez, B.; Calvar, N.; Dominguez, A. J. *Chem. Eng. Data* **2007**, *52*, 1641–1648.
- (11) Torrecilla, J. S.; Raftone, T.; Garcia, J.; Rodriguez, F. *J. Chem. Eng. Data* **2008**, *53*, 923–928.
- (12) Rodriguez, H.; Brennecke, J. F. *J. Chem. Eng. Data* **2006**, *51*, 2145–2155.
- (13) Fröba, A. P.; Wasserscheid, P.; Gerhard, D.; Kremer, H.; Leipertz, A. *J. Phys. Chem. B* **2007**, *111*, 12817–12822.
- (14) Russina, O.; Gontrani, L.; Fazio, B.; Lombardo, D.; Triolo, A.; Caminiti, R. *Chem. Phys. Lett.* **2010**, *493*, 259–262.
- (15) Kelkar, M. S.; Shi, W.; Maginn, E. J. *Ind. Eng. Chem. Res.* **2008**, *47*, 9115–9126.
- (16) Shekaari, H.; Armanfar, E. J. *Chem. Eng. Data* **2010**, *55*, 765–772.
- (17) Singh, T.; Drechsler, M.; Müeller, A. H. E.; Mukhopadhyaya, I.; Kumara, A. *Phys. Chem. Chem. Phys.* **2010**, *12*, 11728–11735.
- (18) Zhang, Q. G.; Wang, N. N.; Yu, Z. W. *J. Phys. Chem. B* **2010**, *114*, 4747–4754.
- (19) Buchfink, R.; Tischer, A.; Patil, G.; Rudolph, R.; Lange, C. *J. Biotechnol.* **2010**, *150*, 64–72.
- (20) Maginn, E. J. *J. Phys.: Condens. Matter* **2009**, *21*, 373101–373114.
- (21) Hanne, C.; Price, S.; Lynden-Bell, R. *Mol. Phys.* **2001**, *99*, 801–809.
- (22) Canongia Lopes, N.; Padua, A. A. H. *J. Phys. Chem. B* **2006**, *110*, 19586–19592.
- (23) Canongia Lopes, N.; Padua, A. A. H. *J. Phys. Chem. B* **2004**, *108*, 16893–16898.
- (24) Canongia Lopes, N.; Deschamps, J.; Padua, A. A. H. *J. Phys. Chem. B* **2004**, *108*, 11250–11250.
- (25) Canongia Lopes, N.; Deschamps, J.; Padua, A. A. H. *J. Phys. Chem. B* **2004**, *108*, 2038–2047.
- (26) Jorgensen, W. L.; McDonald, N. A. *J. Mol. Struct.: Theochem* **1998**, *424*, 145–155.
- (27) Jorgensen, W. L.; McDonald, N. A. *J. Phys. Chem. B* **1998**, *102*, 8049–8059.
- (28) Rizzo, R. C.; Jorgensen, W. L. *J. Am. Chem. Soc.* **1999**, *121*, 4827–4836.
- (29) Price, M. L.; Ostrovsky, D.; Jorgensen, W. L. *J. Comput. Chem.* **2001**, *22*, 1340–1352.
- (30) Cadena, C.; Anthony, J. L.; Shah, J. K.; Morrow, T. I.; Brennecke, J. F.; Maginn, E. J. *J. Am. Chem. Soc.* **2004**, *126*, 5300–5308.
- (31) Wang, J.; Wolf, R. M.; Caldwell, J. W.; Kollman, P. A.; Case, D. A. *J. Comput. Chem.* **2004**, *25*, 1157–1174.
- (32) Liu, Z.; Wu, X.; Wang, W. *Phys. Chem. Chem. Phys.* **2006**, *8*, 1096–1104.
- (33) Liu, X.; Zhou, G.; Zhang, S.; Wu, G.; Yu, G. *J. Phys. Chem. B* **2007**, *111*, 5658–5668.
- (34) Jorgensen, W. L.; Maxwell, D. S.; Tirado-Rives, J. *J. Am. Chem. Soc.* **1996**, *118*, 11225–11236.
- (35) Gontrani, L.; Russina, O.; Lo Celso, F.; Caminiti, R.; Annat, G.; Triolo, A. *J. Phys. Chem. B* **2009**, *113*, 9235–9240.
- (36) Gontrani, L.; Russina, O.; Cesare Marincola, F.; Caminiti, R. *J. Chem. Phys.* **2009**, *131*, 244503–244503.
- (37) Bodo, E.; Gontrani, L.; Triolo, A.; Caminiti, R. *J. Phys. Chem. Lett.* **2010**, *1*, 1095–1100.
- (38) Aoun, B.; Goldbach, A.; Kohara, S.; Wax, J. F.; Gonzales, M. A.; Saboungi, M. L. *J. Phys. Chem. B* **2010**, *114*, 12623–12628.
- (39) Borodin, O.; Gorecki, W.; Smith, G. D.; Armand, M. *J. Phys. Chem. B* **2010**, *114*, 6786–6798.
- (40) Fukuda, S.; Takeuchi, M.; Fujii, K.; Kanzaki, R.; Takamuku, T.; Chiba, K.; Yamamoto, H.; Umebayashi, Y.; Ishiguro, S. *J. Mol. Liq.* **2008**, *143*, 2–7.
- (41) Kanzaki, R.; Mitsugi, T.; Fukuda, S.; Fujii, K.; Takeuchi, M.; Soejima, Y.; Takamuku, T.; Yamaguchi, T.; Umebayashi, Y.; Ishiguro, S. *J. Mol. Liq.* **2009**, *147*, 77–82.
- (42) Umebayashi, Y.; Hamano, H.; Tsuzuki, S.; Lopes, J. N. C.; Padua, A. A. H.; Kameda, Y.; Kohara, S.; Yamaguchi, T.; Fujii, K.; Ishiguro, S. *J. Phys. Chem. B* **2010**, *114*, 11715–11724.
- (43) Macchiagodena, M.; Gontrani, L.; Ramondo, F.; Triolo, A.; Caminiti, R. *J. Chem. Phys.* **2011**, *134*, 114521–114535.
- (44) Russina, O.; Triolo, A.; Gontrani, L.; Caminiti, R. *J. Phys. Chem. Lett.* **2012**, *3*, 27–33.
- (45) Triolo, A.; Russina, O.; Fazio, B.; Appetecchi, G. B.; Carewska, M.; Passerini, S. *J. Chem. Phys.* **2009**, *130*, 164521–164526.
- (46) Triolo, A.; Russina, O.; Bleif, H. J.; Di Cola, E. *J. Phys. Chem. B* **2007**, *111*, 4641–4644.
- (47) Gontrani, L.; Russina, O.; Lo Celso, F.; Caminiti, R.; Annat, G.; Triolo, A. *J. Phys. Chem. B* **2009**, *113*, 9235–9240.
- (48) Russina, O.; Beiner, M.; Pappas, C.; Russina, M.; Arrighi, V.; Unruh, T.; Mullan, C. L.; Hardacre, C.; Triolo, A. *J. Phys. Chem. B* **2009**, *113*, 8469–8474.
- (49) Bodo, E.; Gontrani, L.; Caminiti, R.; Plechkova, N. V.; Seddon, K. R.; Triolo, A. *J. Phys. Chem. B* **2010**, *114*, 16398–16407.
- (50) Russina, O.; Triolo, A. *Faraday Discuss.* **2012**, *154*, 97–109.
- (51) Davila, M. J.; Aparicio, S.; Alcade, R.; Garcia, B.; Leal, J. M. *Green Chem.* **2007**, *9*, 221–232.
- (52) Hardacre, C.; Holbrey, J. D.; Mullan, C. L.; Youngs, T. G. A.; Bowron, D. T. *J. Chem. Phys.* **2010**, *133*, 74510–74517.
- (53) Leskiv, M.; Bernardes, C. E. S.; da Piedade, M. E. M.; N. Canongia Lopes, J. *J. Phys. Chem. B* **2010**, *114*, 13179–13188.
- (54) Canongia Lopes, J. N.; Padua, A. A. H.; Shimizu, K. *J. Phys. Chem. B* **2008**, *112*, 5039–5046.
- (55) Gontrani, L.; Ramondo, F.; Caminiti, R. *Chem. Phys. Lett.* **2005**, *417*, 200–205.
- (56) Gontrani, L.; Ramondo, F.; Caracciolo, G.; Caminiti, R. *J. Mol. Liq.* **2008**, *139*, 23–28.

- (57) Caminiti, R.; Carbone, M.; Panero, S.; Sadun, C. *J. Phys. Chem. B* **1999**, *103*, 10348–10355.
- (58) Caminiti, R.; Carbone, M.; Sadun, C. *J. Mol. Liq.* **1998**, *75*, 149–158.
- (59) Carbone, M.; Caminiti, R.; Sadun, C. *J. Mater. Chem.* **1996**, *6*, 1709–1716.
- (60) Migliorati, V.; Ballirano, P.; Gontrani, L.; Triolo, A.; Caminiti, R. *J. Phys. Chem. B* **2011**, *115*, 4887–4899.
- (61) Smith, W.; Forester, T. R. *J. Mol. Graphics* **1996**, *14*, 136.
- (62) <http://www.cse.clrc.au/msi/software/DLPOLY>, Program version 3.
- (63) Pings, C. J.; Waser, J. *J. Chem. Phys.* **1968**, *48*, 3016–3018.
- (64) J. Z. Yang, a. X. M. L.; Gui, J. S.; Xu, W. G. *Green Chem.* **2004**, *6*, 541–543.
- (65) Jacquemin, J.; Husson, P.; Padua, A. A. H.; Majer, V. *Green Chem.* **2006**, *8*, 172–180.
- (66) Gomez, E.; Gonzalez, B.; Calvar, N.; Tojo, E.; Dominguez, A. *J. Chem. Eng. Data* **2006**, *51*, 2096–2102.
- (67) Fernandez, A.; Garcia, J.; Torrecilla, J. S.; Oliet, M.; Rodriguez, F. *J. Chem. Eng. Data* **2008**, *53*, 1518–1522.
- (68) Matkowska, D.; Goldon, A.; Hofman, T. *J. Chem. Eng. Data* **2010**, *55*, 685–693.
- (69) Del Popolo, M. G.; Voth, G. A. *J. Phys. Chem. B* **2004**, *108*, 1744–1752.
- (70) Bhargava, B.; Balasubramanian, S. *J. Chem. Phys.* **2007**, *127*, 114510–114515.
- (71) Annappareddy, H. V. R.; Kashyap, H. K.; De Biase, P. M.; Margulis, C. *J. J. Phys. Chem. B* **2010**, *114*, 16838–16846.
- (72) Aoun, B.; Goldbach, A.; Gonzalez, M. A.; Kohara, S. K.; Price, D. L.; Saboungi, M. L. *J. Chem. Phys.* **2011**, *134*, 104509–104515.
- (73) Castner, E. W., Jr.; Margulis, C. J.; Maroncelli, M.; Wishart, J. F. *Annu. Rev. Phys. Chem.* **2011**, *62*, 85–105.
- (74) Fujii, K.; Kanzaki, R.; Takamuku, T.; Kameda, Y.; Kohara, S.; Kanakubo, M.; Shibayama, M.; Ishiguro, S.; Umebayashi, Y. *J. Chem. Phys.* **2011**, *135*, 244502–244512.
- (75) Fruchey, K.; Lawler, C. M.; M. D. Fayer, M. *J. Phys. Chem. B* **2012**, *116*, 3054–3064.
- (76) Kashyap, H. K.; Santos, C. S.; Annappareddy, H. V. R.; Murthy, N. S.; Margulis, C. J.; Castner, E. W., Jr. *Faraday Discuss.* **2012**, *154*, 133–143.
- (77) Siqueira, L. J. A.; Ribeiro, M. C. C. *J. Chem. Phys.* **2011**, *135*, 204506–204512.